PCCP

Accepted Manuscript

ROYAL SOCIETY OF CHEMISTRY

www.rsc.org/pccp

Effect of Dispersion on Surface Interactions of Cobalt(II) Octaethylporphyrin Monolayer on Au(111) and HOPG(0001) Substrates: A Comparative First Principles Study

Bhaskar Chilukuri*, Ursula Mazur, K. W. Hipps*

Department of Chemistry, Washington State University, Pullman, Washington 99164-4630, United States

A Density functional theory study of Cobalt(II) Octaethylporphyrin (CoOEP) monolayer on Au(111) and HOPG(0001) surfaces was performed under periodic boundary conditions. Calculations with and without dispersion corrections are performed and the effect of van der Waals forces on the interface properties is analyzed. Calculations have determined that CoOEP molecule tends to bind at the 3-fold and the 6-fold center sites on Au(111) and HOPG(0001), respectively. Geometric optimizations at the center binding sites have indicated that the porphyrin molecules (in monolayer) lie flat on both substrates. Calculations also reveal that CoOEP monolayer binds slightly more strongly to Au(111) than to HOPG(0001). Charge density difference plots disclose that charge is redistributed mostly around the porphyrin plane and the first layer of the substrates. Dispersion interactions cause a larger substrate to molecule charge pushback on Au(111) than on HOPG. CoOEP adsorption tends to lower the work functions of either substrate, qualitatively agreeing with the experimental photoelectron spectroscopic data. Comparison of the density of states (DOS) of the isolated CoOEP molecule with that on gold and HOPG substrates showed significant band shifts around the Fermi energy due to intermolecular orbital hybridization. Simulated STM images were plotted with the Tersoff-Hamann approach using the local density of states, which also agree with the experimental results. This study elucidates the role of dispersion for better describing porphyrin-substrate interactions. A DFT based overview of geometric, adsorption and electronic properties of porphyrin monolayer on conductive surfaces is presented.

Introduction

Porphyrins and metalloporphyrins are promising molecules for numerous chemical, biological and technological applications.[1] Porphyrin based molecules and nanostructures have been used in sensors,[2] molecular electronics,[3] photovoltaics,[4] field effect transistors (FETs),[5] light emitting diodes (LEDs),[6] *etc*. Porphyrins are well known to form self-assembled structures on a variety of substrates.[7-10] Thin films/monolayers of porphyrins on different substrates have been studied by scanning tunneling microscopy (STM) in ambient and ultrahigh vacuum (UHV) conditions.[11] These studies provided considerable insight into structural and electronic properties of individual molecules thus helping to bridge the connection between the molecular and macroscopic world where conventional electronic circuitry is constructed on solid substrates. Principles of higher order organization of molecules may be understood by analyzing the correlation between the structures of molecules and substrates and those of the assemblies thereof.

Numerous scanning probe microscopy studies on porphyrin and phthalocyanine (Pc) based structures[12-20] were performed in our group which led to considerable understanding of their structural, electronic, thermodynamic and self-assembling properties. For example, surface studies on Nickel(II) Octaethylporphyrin (NiOEP) on Au(111) (in UHV)[19] and highly ordered pyrolytic graphite (HOPG)[18, 20] (from benzene and chloroform) have shown that NiOEP molecules pack into similar two-dimensional arrays where the molecules lay flat on the surface, but the lattice constants differ between the Au(111) and HOPG substrates. In another study of oxygen binding to Cobalt(II) Octaethylporphyrin (CoOEP) (Fig. 1) on HOPG substrate,[17] it has been demonstrated that variable-temperature STM can be used to determine adsorption isotherms and thermodynamic data for processes occurring at the solid/solution interface. Those results showed that the lower workfunction (Φ) of HOPG (~4.4 to 5.0 eV)[21-25] led it to act in a manner similar to an electron-donating ligand bound to the fifth coordination site on the cobalt ion of CoOEP, thereby greatly increasing the compound's affinity for oxygen. In contrast, oxygen does not bind strongly to CoOEP supported on Au(111) substrate which has a higher Φ value (5.3 eV).[25] These studies showed the importance of the role of substrate with respect to porphyrin self-assembly and interface chemistry.

A variety of surface studies on metal(II) tetraphenyl porphyrins (MTPP) on various substrates were performed by our group[26-28] and many others as well.[29-34] For example, combined STM, scanning tunneling spectroscopy (STS), x-ray photoelectron spectroscopy (XPS), ultraviolet photoelectron spectroscopy (UPS) and near edge x-ray absorption fine structure (NEXAFS) studies of Cobalt(II) TPP mono and multilayers on Cu, Ag, Au (111) surfaces led to debate[35] about the existence of a valence band at 0.6 eV below the Fermi level in the monolayer but absent in the multilayered CoTPP. It was believed that central metal atom of the metalloporphyrin plays an important role by hybridizing with the metal substrate and forms a band at 0.6 eV below E_F. However, in the multilayered surfaces, no such band is present because of strong interlayer interactions between CoTPP molecules and weak metal substrate interactions beyond the first monolayer. This assumption is further supported by a comparative study of H_2OEP (no metal) and CoOEP monolayers on Ag(111).[35] So to better understand the interfacial chemistry, geometric and electronic properties as a function of adsorbing molecule and the substrate, quantum mechanical simulations can be performed on such interfaces.

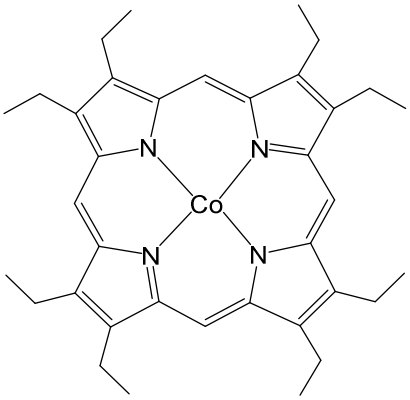

Fig. 1 Molecular structure of Cobalt(II) Octaethylporphyrin

Computational simulations of porphyrin based structures are prevalent in the literature. Most studies involve the application of molecular quantum mechanical codes on single porphyrin molecules and its derivatives to understand and rationalize the various experimental findings. However, as listed in the previous examples, the substrate plays a significant role in altering the

chemical and electronic properties of the porphyrin deposited on it. So, periodic simulations of porphyrin adlayers on different substrates are necessary to correctly describe the state of adsorbed porphyrins. Computational modeling under periodic boundary conditions has been performed on a wide variety of porphyrin derivatives and substrates. For example, many first principles electronic structure calculations were performed to determine the saddling or geometric orientation of TPP derivatives on different substrates.[29, 36, 37] Calculations at different orientations of the phenyl substituents helped in explaining the typical monolayer formations on the substrates which are responsible for their unique properties. Periodic simulations of various porphyrin derivatives on substrates like Cu(110),[38, 39] Au(111),[40-43] Ag(111)[44] and HOPG[45, 46] were performed to determine their interfacial geometries, adsorption energetics, electronic properties and to support the corresponding experimental findings. A variety of computational studies were done to explain the magnetic and sensing properties[47, 48] of various porphyrin derivatives for applications in spintronic and sensor devices respectively. Recently, molecular dynamics simulations were performed on monolayer formation characteristics of porphyrin derivatives on different substrates.[49, 50]

Most of the early DFT studies[38-42, 51] performed on porphyrin-substrate junctions were done using LDA and GGA functionals which tend to underestimate the dispersion interactions between the adjacent porphyrin molecules and with the substrate. This led to very low adsorption energies. Hence dispersion corrected DFT methods like DFT-D[52, 53] and vdW-DF[54] have gained considerable attention due to their better description of van der Waals forces and thus better energies and good comparison with experimental data. Many studies of small conjugated molecules on metal substrates have been performed using dispersion corrected DFT, but few of them on porphyrin based structures and none that we know about for porphyrins on Au(111) and HOPG substrates. In this paper, we report a comprehensive computational study on geometric, adsorption and electronic properties of cobalt(II) octaethylporphyrin (CoOEP) monolayer (Fig. 1) on Au(111) and highly ordered pyrolytic graphite (HOPG) 0001 surfaces. All simulations were performed under periodic boundary conditions using density functional theory (DFT) with and without dispersion corrections. Furthermore, data obtained from theoretical modeling is compared with experimental findings.

Computational Methodology

All simulations were performed using the Vienna *Ab initio* Simulation Package (VASP)[55-57] version 5.2. Periodic calculations were performed using plane-wave density functional theory (PW-DFT) within the projector augmented wave (PAW)method[58, 59] to describe the core electrons and valence–core interactions. For non-dispersion calculations, generalized gradient approximation (GGA)[60] exchange–correlation functional of Perdew, Burke and Ernzerhof (PBE) was employed on Au(111) systems and local density approximation (LDA)[61]correlationfunctional was used on HOPG(0001) systems. Dispersion DFT calculations were done with vdW-DF method[54, 62, 63] which takes into account the nonlocal nature of electron correlation. For the Au(111)-porphyrin system, the optB88-vdW GGA functional with PBE potentials having p, s semicore valence for Au and Co atoms was used. For the HOPG-porphyrin system, the vdW-DF LDA functional with PBE potentials having s semicore valence for the Co atom was used. Calculations for isolated CoOEP molecules were carried out with either functionals in conjunction with the respective substrates.

The choice of the DFT functionals was based on comparison of optimized lattice constants and bulk modulus[25] of *fcc*-gold and HOPG unit cells with their crystal structures. The aforementioned functionals were able to predict the geometries relatively well with < 0.02 Å error in their respective lattice constants. We also performed some calculations of HOPG surface with optB88-vdW GGA functional for energy comparisons (details later in the paper) and noted that GGA overestimates lattice constants of HOPG in the c-lattice direction by about 0.80 Å, hence all calculations on HOPG systems were done with LDA and Au(111) systems with GGA unless mentioned otherwise.

For slab calculations, the electronic wave functions are sampled in a k-point grid of 3×3×1 for Au(111) systems and 2×2×1 for HOPG(0001) systems in the irreducible Brillouin zone (BZ) using the Monkhorst and Pack (MP)[64] method. Isolated CoOEP molecules were sampled with only a gamma point. Plane wave cut off energies of 450 eV and 550 eV were used for gold and HOPG systems, respectively, and these values were determined from energy convergence tests on their respective primitive lattices. Methfessel–Paxton smearing was used to set the partial occupancies for each wave function with a smearing width of 0.2 eV. Finally, constant current STM images were simulated using the Tersoff-Hamann[65, 66] approach implemented in the bSKAN code.[67] This code uses the electron wave functions of the slab computed previously with VASP.

Simulation Model

To model the interface interactions between the CoOEP monolayer and gold or HOPG substrates, appropriate initial geometries are necessary. The guess structures for the simulation were based on previously obtained experimental data and molecular DFT calculations. A detailed description of how the initial structures were guessed and built is given below.

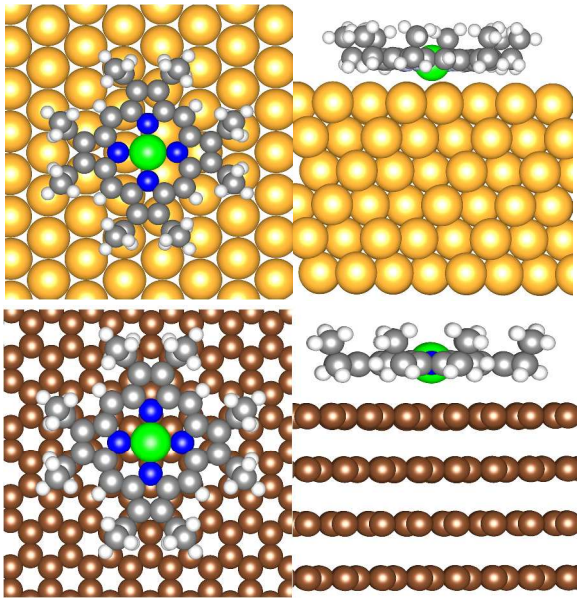

Fig. 2 Optimized geometries of CoOEP molecule on Au(111) (on top) and HOPG(0001) surfaces (bottom). Images on the left and right depict the top and side views respectively. Atom colors: Porphyrin carbon-grey, nitrogen-blue, hydrogen-white. Gold and HOPG-carbon atoms are colored in yellow and brown respectively.

a) Au(111) and HOPG Surfaces: Crystal structure unit cells[68] of *fcc*-gold and HOPG were optimized with plane-wave DFT and were used to build their respective (111) and (0001) surfaces. The primary surfaces of Au(111) and HOPG(0001) were multiplied $6 \times 6 \times 2$ and $8 \times 8 \times 2$ in *a, b, c* directions respectively to obtain super cells with lattice parameters listed in

Table 1. A vacuum of ~30 Å is added along the c direction for creating a more realistic slab structure for Au(111) and HOPG(0001). Surface reconstruction effects are ignored for all the calculations due to their negligible effects on the monolayer adsorption properties as determined from experimental observations.

b) Cobalt(II) Octaethylporphyrin (CoOEP) Monolayer: Experimental STM images of CoOEP monolayer on Au(111)[69] and HOPG[17] shows that all the 8 ethyl substituents on the porphyrin stay in an "all up" or "crown" configuration instead of the packing seen in the crystal structure.[70] So a molecular geometry of "all up" CoOEP was built and optimized using molecular DFT calculation previously.[17] The optimized geometry obtained from gas phase molecular calculation was used as the starting geometry for the present study. The lattice parameters for modeling the isolated CoOEP molecule are listed in Table 1, where the CoOEP molecule is placed at the center of the cubic box.

Table 1. Lattice parameters of Au, HOPG slabs, Au(111)/HOPG–CoOEP interface systems and isolated CoOEP molecule.

System	*a* (Å)	*b* (Å)	*c* (Å)	*α* (°)	*β* (°)	*γ* (°)
Au(111) and Au(111)/CoOEP	17.61	17.61	52.38	90	90	120
HOPG(0001) and HOPG/CoOEP	19.57	19.57	47.39	90	90	120
Isolated CoOEP	30	30	30	90	90	90

c) CoOEP and Au(111)/HOPG Interface: A single CoOEP molecule is placed on the top of optimized $6 \times 6 \times 2$ and $8 \times 8 \times 2$ slabs of Au(111) and HOPG(0001) respectively, thus transferring the cell parameters of the slabs to the interfaces (Table 1). The proposed slab model with single CoOEP molecule per unit cell represents a monolayer packing density of ~83% on Au(111) and ~75% on HOPG(0001) under the given substrate parameters, while avoiding strong intermolecular repulsions between hydrogen atoms of the ethyl substituents from neighboring molecules. Although the exact size of the unit cell of the proposed model differs from experiment,[17-20] the effect of this difference should be negligible considering monolayer coverage density of ~77% (1.88 nm^2/molecule) for similar porphyrin (NiOEP) molecule on Au(111) surface[19] obtained from UHV-STM studies. Additionally, experimentally obtained porphyrin monolayer pattern indicates considerable separation between ethyl substituents (*i.e.,* weak intermolecular interactions)[19] of neighboring porphyrin molecules which is consistent with the proposed model.

Results and Discussion

a) Binding Site: All possible adsorption sites for CoOEP molecule on Au(111) and HOPG(0001) surfaces are examined (details in Supporting Information) to determine the stable binding site. Calculations indicated that CoOEP is relatively stable at the 3-fold and 6-fold center sites with porphyrin nitrogen atoms preferring the planes along top and bridge sites upon symmetrical rotation, Fig.2. However, we see very small differences in computed energies (< 0.2 eV, Table S1) at different binding sites. This could be due to relative shortcomings in theoretical accuracy and symmetrical constraints in the present model. So it is prudent to assume that CoOEP molecules may prefer different binding sites governed by intermolecular interactions than substrate-adsorbate interactions (with respect to energetics) under experimental conditions (like solvation, high temperature).[43] However, for modeling purposes, we chose the theoretically obtained low energy adsorption sites at 3-fold and 6-fold centers for Au(111) and HOPG systems.

b) Optimized Geometries: Geometry relaxations of all systems described in the simulation model were carried on with LDA, GGA and vdW-DF functionals. *For comparative purposes, we present the optimized geometric parameters with and without (in the parenthesis) dispersion functionals*. Each layer in the fully relaxed slabs of Au(111) and HOPG(0001) remains extremely flat with averaged inter layer separations of 2.32 (2.40) and 3.32 (3.33) Å respectively. In the Au(111) slab, the averaged Au-Au bond distances are 2.90 (2.93), while the averaged C-C distances in HOPG(0001) are found to be 1.41 (1.41). Overall, the geometries of optimized slabs agree closely with their respective crystal structures.[68] Inclusion of dispersion correction led to an interlayer geometrical variation of ~0.10 Å in Au(111) contrary to HOPG (~ 0.00 Å) where no variation is seen. This confirms the existence of larger dispersion interactions in gold than in HOPG.

A CoOEP molecule having initial geometry obtained from molecular DFT calculations[17] is placed in a cubic box of 30×30×30 Å and fully relaxed. The enormous size of the box is selected to avoid any periodic interactions between neighboring molecules and thus obtaining an optimized structure of an isolated CoOEP molecule. The optimized geometry from plane-wave DFT calculation (Fig. S2 through S4) is mostly similar to the one obtained with the molecular hybrid-DFT calculations,[17] but the Co-N bonds vary by ~0.05 Å. The LDA functional with and without dispersion corrections underestimate the Co-N bond lengths by ~0.03 Å, while GGA functional without the dispersion corrections seems to overestimate the Co-N bond lengths by ~0.03 Å, relative to molecular hybrid-DFT calculations. But, C-C and C-N bonds are similar irrespective of the functional used. Among all the CoOEP geometries (Fig. S2 through S4), the geometry obtained with vdW-DF B88-GGA functional resembled closely the molecular hybrid-DFT calculations.[17]

Initial geometries of CoOEP-Au(111)/HOPG interfaces were constructed from the optimized geometries of CoOEP, Au(111) and HOPG(0001). Instead of optimizing at all the possible binding sites of CoOEP on Au(111)/HOPG, low energy binding site geometries *i.e.*, CoOEP on the 3-fold and 6-fold center sites of Au(111) and HOPG(0001) respectively were optimized. The optimization is carried out by freezing the bottom 3 layers for the gold slab in CoOEP-Au(111) system and the bottom 2 layers for CoOEP-HOPG(0001) system. Upon relaxation, the top layer of HOPG buckles slightly away from the porphyrin. In Au(111), the top layer remains nearly flat but gold atoms closer to the porphyrin metal and nitrogens are disturbed from being completely flat. This may indicate a weak interface dipole formation which we will explain in the later part of the article. The rest of the substrate layers in both substrates remained mostly flat nearly retaining the geometry as in the respective non-adsorbate slabs. The average distance between adsorbate and graphite surface was found to be 3.20 (3.37) Å. On Au(111) the distances were 2.93 (3.25) Å. The geometry of CoOEP molecule on both Au(111) and HOPG(0001) remains similar to that of the isolated molecule optimized in the cubic box. This indicates that the deposition of CoOEP monolayer on Au(111) and HOPG(0001) does not significantly impact the geometric integrity of either surface thus forming a stable interface.

c) Adsorption Energies: The adsorption/binding energy of an CoOEP on gold and HOPG substrates can be obtained from the following equation

$$E_{ads} = E_{S\text{-}P} - [E_S + E_P] \quad (1)$$

In equation (1), E_{ads} represents the CoOEP adsorption energy and $E_{S\text{-}P}$, E_S, E_P represents the total energies of individually optimized substrate-porphyrin complex, clean substrate and isolated porphyrin molecule respectively. The actual adsorption energy (E_{ads}) is a combination of electronic (E_{elec}) and vibrational (E_{vib})

energies. Since the vibrational components are much lower than the electronic components, phonon calculations are not performed and hence neglected.[71-75] Without the dispersion corrected DFT functional, the calculated adsorption energies from electronic components of CoOEP on Au(111) and HOPG(0001) were found to be -0.31 and -1.18 eV respectively. These energies indicate that CoOEP binds relatively stronger to HOPG than on Au(111). At this juncture, one should consider that GGA severely underestimates (by ~60%) the intermolecular interaction energies while LDA overestimates them (by ~30%).[76] However, the calculated electronic adsorption energies (E_{ads}) are also much lower than the experimental enthalpy of sublimation ($\Delta_{sub}H_m$), 1.00±0.13 eV for CoOEP complexes.[77] It is important to note that enthalpy of adsorption (ΔH_{ads}) for CoOEP monolayer on a substrate should always be $\geq \Delta_{sub}H_m$. We attribute the anomaly in the calculated and experimental values mostly to underestimation of dispersion interactions by regular DFT (both GGA and LDA) calculations and slightly to the vibrational component of the adsorption energies. Calculations with vdW-DF dispersion corrected DFT functional yielded CoOEP adsorption energies of -4.34 and -2.42 eV on Au(111) and HOPG surfaces respectively. This binding trend is opposite to that seen with non-dispersion calculations but expected considering that the dispersion in Au atoms is much stronger[78] than on graphite. The stronger adsorption energies with dispersion calculations are qualitatively consistent with what is observed for similar supramolecular building blocks on metal[79, 80] and graphite[81, 82] surfaces, obtained both experimentally and theoretically.[43, 79] For example, the calculated dispersion corrected adsorption energy for vanadyl naphthalocyanine (VONc) on Au(111) surface is reported as -5.5 eV[43]. The higher adsorption energy for VONc can be attributed to its larger surface area.[83] We also performed additional calculations using dispersion corrected DFT-D3 by Grimmie *et. al.*, on the same geometries obtained from vdW-DF calculations, to account for the van der Waals effect. E_{ads} for CoOEP/Au(111) and CoOEP/HOPG systems upon dispersion corrections were found to be -4.92 eV and -3.03 eV respectively. Both vdW-DF and DFT-D3 methods produce a similar trend in adsorption energies. The small discrepancy in the values of adsorption energy can mostly be attributed to non-optimization of geometries with DFT-D3 and overestimation by DFT-D method.[78]

Table 2. Adsorption energies of CoOEP on Au(111), HOPG and other notable adsorbate-substrate systems cited in this paper. Superscripts refer to literature citations. 'Calculated' column refers to dispersion DFT and non-dispersion DFT (in parenthesis) calculated adsorption energies.

Adsorbate	Substrate	Calculated (eV)	Experiment (eV)
CoOEP	Au(111)	-4.34 (-0.31)	
CoOEP	HOPG	-2.42 (-1.18)	
PTCDA	Au(111)	-1.88 [a]	2.00 [b]
NTCDA	Au(111)	-1.31 [a]	1.50 [b]
Vanadyl Pc[43]	Au(111)	-5.50	
Iron Pc[84]	HOPG, Au(110)		2.8 ± 0.1, > 3.2 ± 0.1
Iron Pc, Cobalt Pc, Copper Pc[85]	Graphene on Ir(111)		3.20, 3.20, 3.60

[a] Reference [86], [b] Reference [83]

We made two interesting observations upon analyzing the adsorption energies. First, the calculated adsorption energy of CoOEP (-4.34 eV) is greater than PTCDA (-1.88 eV)[86] on Au(111) surface. It is important to point out that although CoOEP and PTCDA have a similar conjugated bond structure and are similar in size, larger adsorption energy is observed for CoOEP. Due to lack of experimental data for CoOEP/Au(111) system, we compare the adsorption energies to a structurally similar PTCDA/Au(111) system using similar computational methodology. Note that the dispersion DFT calculations performed on PTCDA/Au(111) system[86] are similar to that used in the present study of CoOEP/Au(111) system. Calculated adsorption energy[86] for PTCDA/Au(111) (-1.88 eV) is also comparable its respective experimental value (2.00 eV).[83] These findings strengthens the fact that the current theoretical methods were aptly chosen and would predict binding energies similar to experiment. *Hence, we attribute the higher adsorption energy for CoOEP mostly to the presence of the transition metal cobalt contrary to structurally similar PTCDA*. This attribution is consistent with recent experimental desorption study[85] of different metal-phthalocyanines on surfaces which reports that transition metals significantly alter the adsorption energies on surfaces.[85]

The second interesting observation is that porphyrins bind more strongly to Au(111) than on HOPG(0001). One would wonder if this comparison is justified considering the computed adsorption energies on Au(111) and HOPG(0001) are obtained using two different DFT functionals, GGA and LDA respectively. In order to justify our comparison, we performed similar calculations of CoOEP/HOPG system with vdW-DF B88-GGA functional and obtained an adsorption energy of -2.94 eV, hence *we conclude that irrespective of the functional used porphyrins bind more strongly to Au(111) than on HOPG(0001)*. These values are consistent with the recent experimental study[84] of adsorption of iron-phthalocyanine (FePc) on HOPG and Au(110). It was reported that the FePc (structurally similar to CoOEP) single layer has a larger adsorption energy on Au(110) (> 3.2 eV) than on HOPG (2.8 eV). We note that the adsorption energy on Au(111) would be even higher due to its smaller surface energy[87] than Au(110). This finding is particularly interesting considering our earlier study of temperature dependent adsorption-desorption properties of porphyrins in phenyloctane/Au(111) solution-solid interface.[16] In this study it was shown that at low temperatures, desorption of CoOEP and NiOEP porphyrins from Au(111) surface is completely dependent on kinetics rather than on thermodynamics, but that could change at high temperatures. It was also shown that porphyrins due to their large van der Waals interactions bind more strongly to Au(111) than covalently bonded thiols. Considering the adsorption energies obtained from present calculations, *we predict that desorption of porphyrins on HOPG surface may occur at lower temperatures than that seen on Au(111)*. This could be due to weaker interactions of porphyrins with HOPG than on Au(111). Note that solvation of porphyrin molecules and substrate by phenyloctane also plays an important role in aiding the desorption process which is not considered in the present calculation. But we are confident that solvation energies would be <<1.9 eV (calculated difference in adsorption energies of CoOEP on gold and HOPG substrates) and should not alter the adsorption/desorption trend. Thus, we predict a substrate dependence on the adsorption-desorption properties of porphyrins.

d) Charge Redistribution: Deposition of molecules of CoOEP on both HOPG and Au(111) surfaces leads to charge redistribution due to electronic hybridization between the orbitals of the adsorbate and the adsorbent. The local charge density (CD) in the z-direction can be obtained by plane-averaging the one dimensional Poisson's equation over the *xy*-plane. The local charge density difference is given as follows

$$\rho_{diff}(z) = \rho_{S-P}(z) - \rho_S(z) - \rho_P(z) \qquad (2)$$

In equation (2) $\rho_{diff}(z)$ is the plane (x,y) averaged charge density (CD) difference in the z-direction and $\rho_{S\text{-}P}(z)$, $\rho_S(z)$, $\rho_P(z)$ are the plane averaged charge densities for the optimized substrate-porphyrin complex, substrate and porphyrin monolayer

respectively. Note that the charge densities for the substrate and porphyrin monolayer are obtained from exactly the same geometries as in the substrate-porphyrin complex. The plane-averaged CD difference (with and without dispersion DFT) in the z-direction for CoOEP/Au(111) and CoOEP/HOPG systems are given in left panels of Fig. 3, 4. Three dimensional (3D) images of charge redistribution at the interfaces of CoOEP/Au(111) and CoOEP/HOPG systems are given in right panels of Fig. 3, 4.

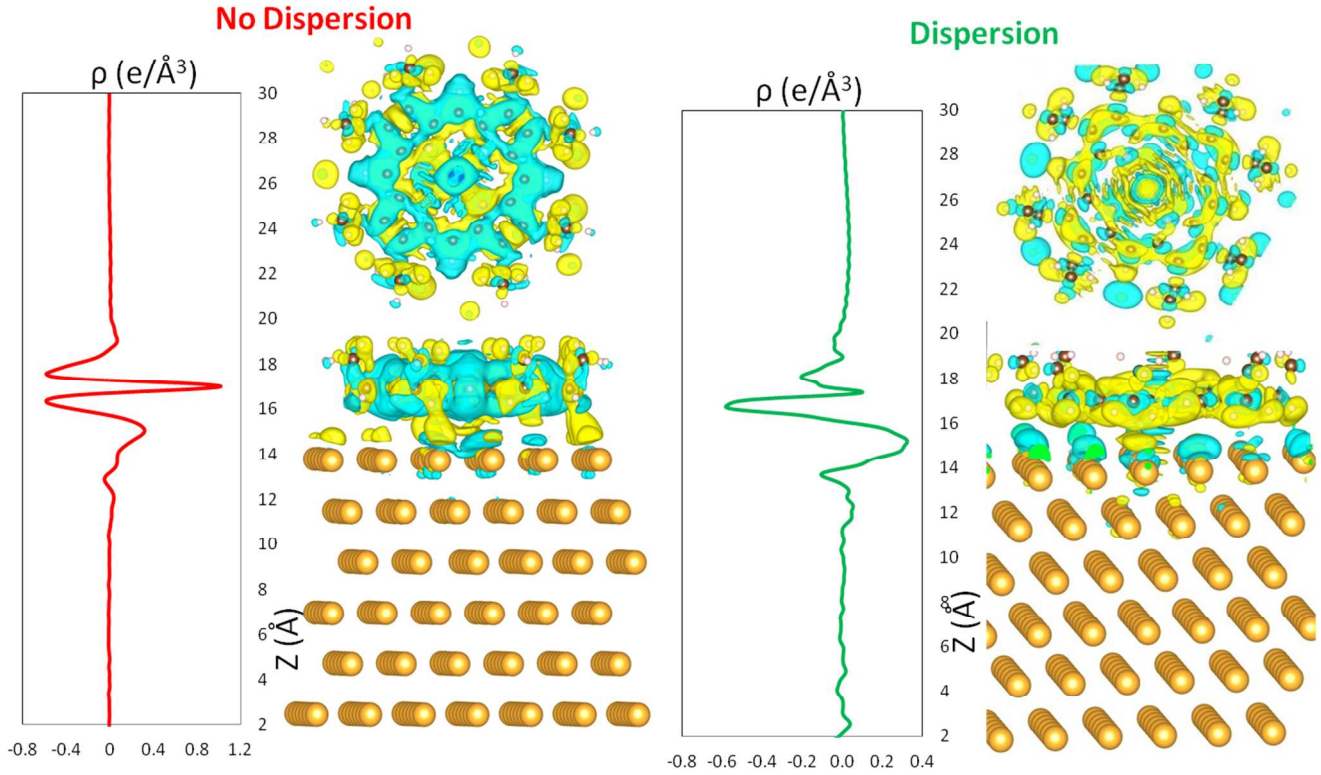

Fig. 3 Charge density difference for CoOEP/Au(111) system without (left) and with (right) dispersion. For each image, plot on the left is the x-y plane averaged charge difference, with charge density (ρ) on the x-axis and distance (Å) in z-direction of the interface unit cell on y-axis. Figure on the right represents the 3 dimensional iso-density (+ve: yellow and –ve: cyan) of charge density difference.

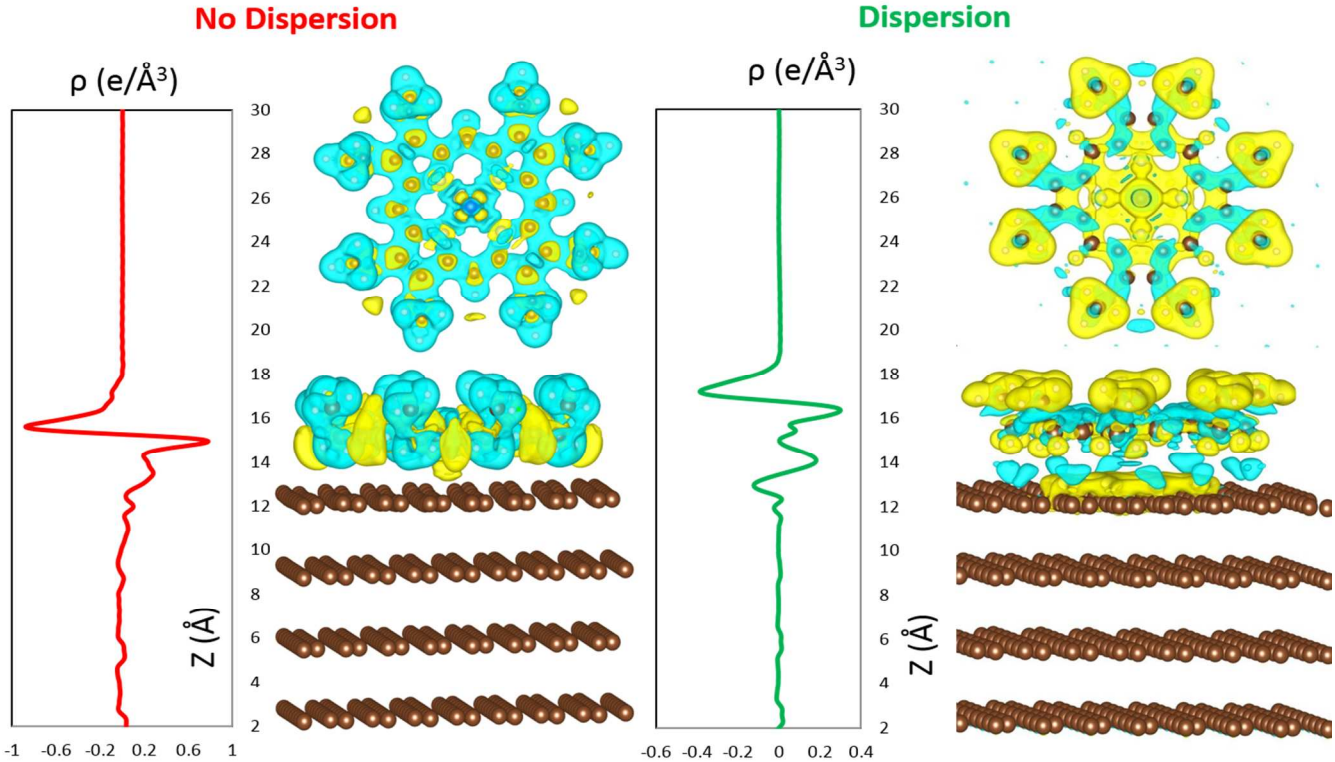

Fig. 4 Charge density difference for CoOEP/HOPG(0001) system without (left) and with (right) dispersion. For each image, plot on the left is the x-y plane averaged charge difference, with charge density (ρ) on the x-axis and distance (Å) in z-direction of the interface unit cell on y-axis. Figure on the right represents the 3 dimensional iso-density (+ve: yellow and –ve: cyan) of charge density difference.

With GGA-PBE functional, the plane (*xy*) averaged charge redistribution in CoOEP/Au(111) interface (Fig. 3, left) plotted as a function of distance along z-direction of interface unit cell show that, charge density difference fluctuates from nearly zero at 5th layer (from bottom) of gold slab to +ve region on the 6th layer followed by significant –ve shift in between the CoOEP molecule and the top of Au(111) slab. On the CoOEP, the CD difference was mostly +ve on the porphyrin molecular plane but it turns –ve on the ethyl substituents. The integrated charge density difference yields a net metal-to-molecule charge redistribution of -0.2*e*. The 3 dimensional iso-surfaces (Fig. 3, left) of charge redistribution at the interface indicates that the charge was localized mostly on the porphyrin plane with smaller amounts on the top layer of Au(111) and on ethyl substituents on the porphyrin. With dispersion corrected DFT, charge density difference (Fig. 3, right) fluctuates from nearly zero at 5th layer (from bottom) of gold slab to +ve region layer until it nears the CoOEP molecule. On CoOEP, the CD difference was mostly -ve with a slight dip towards zero between the porphyrin plane and the ethyl substituents. The integrated charge density difference yields a net metal-to-molecule charge redistribution of -2.0*e*. The 3 dimensional isosurfaces (Fig. 3, right) of charge redistribution at the interface indicates that the combined charge was localized mostly on the porphyrin plane with considerable amounts on the top layer of Au(111) as well.

In the CoOEP/HOPG system, plane (*xy*) averaged charge redistribution (Fig. 4, left) at the interface with and without dispersion looks to be remarkably similar. With both functionals, the charge density difference fluctuates from zero at the bottom of HOPG slab to +ve region at the top layer of HOPG to the porphyrin plane. A -ve shift is seen on the ethyl substituents. The integrated charge density difference yields a net substrate-to-molecule charge redistribution of about 0.4e and 0.6e with and without dispersion respectively. This phenomenon is also reflected in the 3D images of CD redistribution (Fig. 4, right). The iso-surfaces of charge redistribution at the interface indicate that the combined charge was localized on the porphyrin plane and its substituents contrary to the case on Au(111) slab where significant charge is also localized mostly on the porphyrin plane rather than on its substituents. Due to inclusion of dispersion interactions, the amount of charge redistribution is significantly more on gold than on HOPG. Greater charge redistribution in Au(111) systems is possibly due to shorter CoOEP-gold distance caused by higher dispersion forces contrary to CoOEP-HOPG system. Overall, a so called '*push-back effect*'[88] is observed on either surface, indicating charge localization mostly toward the porphyrin rather than toward the substrate. Another significant finding from the charge redistribution analysis is that *dispersion interactions play a significant role in altering the charge redistribution on Au(111) than on HOPG*.

e) Workfunctions: Numerous studies both experimental[89-92] and theoretical[93-98] have shown that adsorption of organic molecules on conducting substrates causes changes to the energy level alignments and workfunctions (Φ). In order to determine the corresponding changes we calculated the Φ values for clean Au(111), HOPG substrates and when CoOEP monolayer is deposited on them. For comparative purposes, we report the Φ values with and without dispersion interactions. In this section, the value in the parenthesis refers to non-dispersion functional. Calculated Φ for clean Au(111) and HOPG were determined to be 5.11(5.21) eV and 4.61(4.55) eV respectively. These values closely agree with their respective experimental work functions.[25] Upon CoOEP molecule adsorption, the calculated workfunction of CoOEP/Au(111) and CoOEP/HOPG(0001) systems were found to be 4.35(4.74) eV and 3.98(4.27) eV respectively. In both cases the respective Φ values are lowered in contrast to clean substrates and is consistent with CoOEP/Au(111) UPS spectra.[34] Although intrinsic shortcomings of current DFT methodology[99, 100] could prevent a full quantitative comparison with experimental UPS data, we are confident that a qualitative picture can be established. Experimental spectroscopic studies have shown that the central metal atom plays a significant role in the workfunction changes.[35] The workfunction changes can be attributed mostly to the formation of interface dipoles caused by Pauli repulsion[88] between the occupied states of the molecule and the substrate leading to a mutual polarization and smaller changes in the vacuum energies.[94, 101, 102] Calculated surface dipole energies for CoOEP/Au(111) and CoOEP/HOPG(0001) systems were determined to be 0.60(0.41) and 0.35(0.23) eV respectively. *DFT with and without dispersion yields similar qualitative results but dispersion interactions resulted in larger interface dipoles and Φ difference on either substrate than without London forces.*

f) Energy Level Alignments and Density of States: Porphyrins have wide applications in numerous technological devices and a key element to their application is their energy level alignment when isolated and in conjunction with an electrode in a device. Density of states (DOS) of isolated CoOEP molecule is calculated with dispersion and non-dispersion GGA and LDA DFT functionals mentioned in the methodology section (Fig. 5, S5). Comparison of DOS of the isolated molecule with different functionals did not yield different relative positioning of the projected density of states (pDOS) and produced a similar band gap of ~1.3 eV with all the functionals. So due to the aforementioned reasons and for simplicity we only discuss the DOS of the isolated molecule obtained from vdW-DF GGA functional. Figures 5-6 and S5-S10 show the calculated density of states (DOS) of isolated CoOEP and its monolayers on Au(111) and HOPG(0001), respectively. The calculated Fermi energy (E_f) (i.e., top of valence band and not to be confused with Fermi level) was set to zero (eV) for all DOS plots. For the isolated molecule (Fig. 5), the band gap is ~1.3 eV. The top of the valence band is dominated by the cobalt metal atom, mostly by d_{xz}, d_{yz} and d_{z^2} orbitals with some contribution from the carbon p_z orbitals (Fig.S6). Also, nitrogen atom contributions are very low in the valence band in comparison to the carbon and cobalt atoms. On the other hand, the bottom of the conduction band is predominantly populated by the carbon p_z orbitals with some contributions from the nitrogen p_z and cobalt d_{xz}, d_{yz} orbitals. From the DOS of isolated CoOEP molecule, it is important to note that after the energy level (~ +1.35 to +1.85 eV) at the bottom of the conduction band, the next level is nearly 0.4 eV above it. This energy level alignment changes upon adsorption of the CoOEP molecule on a substrate. As we will report next, the adsorption of CoOEP monolayer on the substrates causes significant hybridization leading to creation of new states both in the valence and conduction bands not seen in the isolated CoOEP molecule.

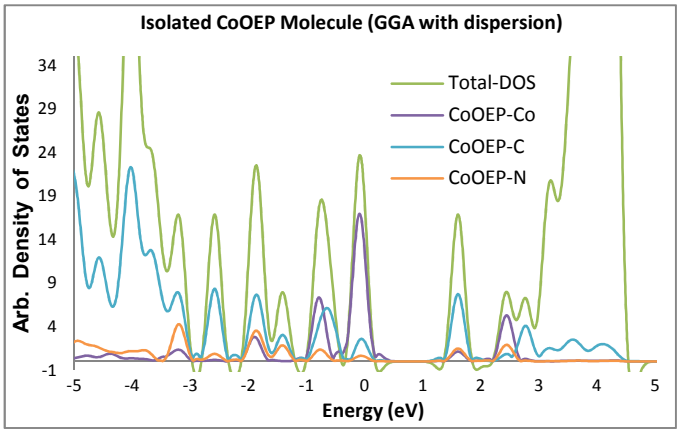

Fig. 5 Density of States (DOS) for isolated CoOEP molecule. Fermi energy is aligned to 0 eV.

Density of states of CoOEP monolayer on Au(111) and HOPG(0001) with and without dispersion are depicted in Figures 6, S7-S10. In the HOPG(0001) system, when DOS is compared between non-dispersion (Fig. S9) and dispersion (Fig. 6, bottom) calculations, the positioning of projected density of states (pDOS) does not change significantly. But in Au(111) system, similar comparison, yields different pDOS especially in the relative amount (i.e., peak height/area under curve) of cobalt orbitals but not their positioning in the energy scale (see Fig. S8). However the height/area, the positions of these DOS in the energy scale remain similar with and without dispersion corrections. For equivalent comparison we will focus the rest of our discussion in this paper to compare the DOS of isolated CoOEP molecule with the respective monolayers on Au(111) and HOPG(0001) obtained using vdW-DF calculations.

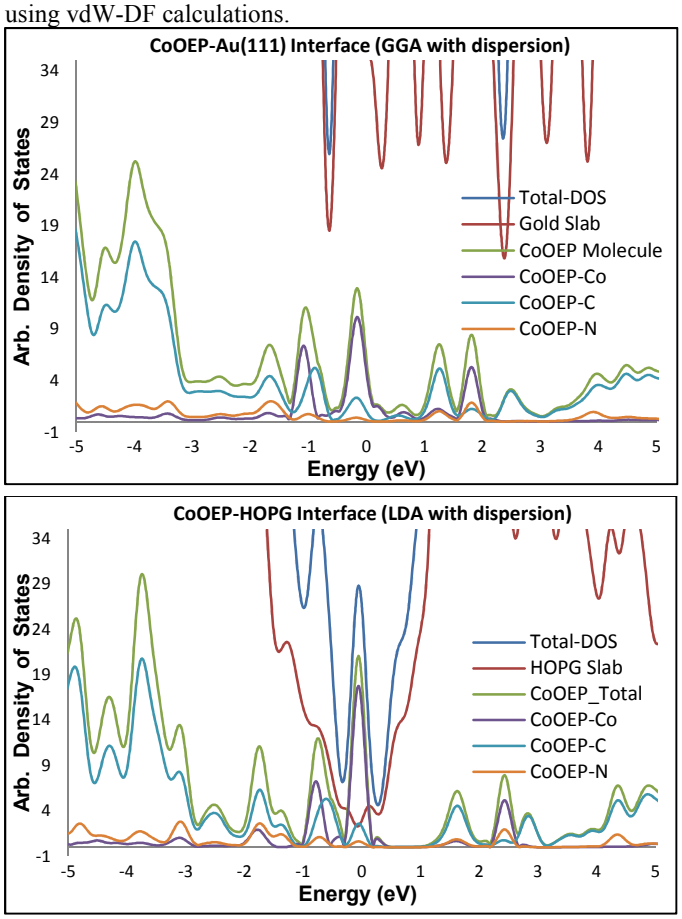

Fig. 6 Density of States (DOS) for CoOEP/Au(111) (top) and CoOEP/HOPG (bottom) systems. Fermi energy is aligned to 0 eV.

The projected density of states (pDOS) of CoOEP monolayer on Au(111) surface (Fig. 6 (top), S8 (left)) indicate that the top valence band is populated mostly by the cobalt metal atom (d_{z2}, d_{xz}, d_{yz}) followed by the carbon atom (p_z). A minor contribution from the nitrogen p_z orbitals is also seen in the top of valence band. All projected orbital contributions for CoOEP monolayer on Au(111) are given in Fig. S8. Above the Fermi energy, some additional DOS states with partial occupancy (i.e., < 1 e^-) were seen between ~ +0.4-0.8 eV due to broadening of Co-d_{z2} and carbon p_z orbitals. These states could be *metal-induced-gap-states*[103-105] which were not present in the isolated CoOEP molecule (Fig. 5). Interestingly, these states were insignificant in CoOEP-HOPG system (Fig. 6, bottom). We think that these new gap states could aid the larger '*push-back effect*' (Fig. 3, right) seen between the porphyrin and Au(111) when dispersion interactions are included in the calculations. The bottom of the conduction band (i.e., empty states) has 2 consecutive bands, the first band (+1.0-1.6 eV) mostly populated by carbon, nitrogen p_z orbitals with some cobalt d_{xz}, d_{yz} orbitals and the second band (+1.6-2.0 eV) contributed by cobalt d_{x2-y2}, d_{xy} with some nitrogen p_x, p_y and s orbitals. Comparing the DOS of isolated CoOEP molecule (Fig. 5) and its monolayer on Au(111) (Fig. 6, top) around the Fermi energy (E_f) primarily show the shift in 2 bands. First, the upward shift in carbon-p_z orbitals creates a shoulder at ~ -0.8 eV (due to band broadening) in the valence band of CoOEP/Au(111). The other band at +1.6-2.0 eV in CoOEP/Au(111) system which shifted downwards from +2.2-2.7 in isolated CoOEP molecule. Although the band positions obtained from DFT cannot exactly be matched with experimental UPS spectra, one can compare the relative positions of the bands.[99, 100] We attribute the mid-gap state seen in the calculated DOS of CoOEP/Au(111) at 0.2eV to the additional band observed at in experimental UPS data[35] of Co porphyrin on Au(111). In the present comparison, the new band seen in the experimental UPS data[35] is the first band below the Fermilevel and in the mid-gap area with respect to clean Ag(111). This new band is comparable to similar mid-gap band at 0.2 eV in the calculated DOS.

Projected density of states (pDOS) of CoOEP monolayer on HOPG (Fig. 6 (bottom), S10 (right)), looks similar to that on Au(111) surface but with no CT states. The basic difference between either substrates is the sharp decline in the total DOS near the Fermi energy in HOPG substrate consistent with experimental DOS of HOPG.[106] Like on Au(111), the top valence band is populated mostly by the cobalt metal atom followed by the carbon atom and minor contributions from the nitrogen orbitals are also seen. The bottom of the conduction band has 3 consecutive bands populated mostly with carbon orbitals (+1.1-2.2 eV) followed by cobalt d_{x2-y2}, d_{xy} orbitals (+2.2-2.6 eV) and carbon-p_z orbitals (+2.6-3.1). Similar to Au(111) interface, CoOEP/HOPG (Fig. 6, bottom) also show a shift in 2 bands around E_f when compared with isolated CoOEP molecule (Fig. 5).The primary band shifts are located at -0.5 eV (shoulder due to shift carbon-p_z) and +1.9-2.2 (due band broadening) which were absent in the isolated CoOEP (Fig. 5,S6). Interestingly, the shift in the conduction band is different from that observed in CoOEP/Au(111) interface.

In summary, calculated DOS of cobalt(II) octaethylporphyrin when isolated and when on substrates vary significantly indicating some electronic interactions between the monolayer and substrates. Orbital projections from DOS also helped with better understanding of the experimental data obtained from UPS and STS on different porphyrin monolayers. We will show in the next section of how the pDOS data can be used to predict the experimental and simulated STM images.

g) STM Images: Scanning tunneling microscopy (STM) images are simulated using the Tersoff-Hamann approach,[65, 66] which assumes that tunneling current is proportional to the local density of states (LDOS) at the position of the STM tip and only the orbitals localized at the outermost tip atom will be of importance for the tunneling process. So the simulated STM images were obtained by assuming the outermost tip atom to be an atomic *s*-wave-function. Constant current STM images can be plotted from partial charge density (obtained from VASP) at any given energy (bias voltage) but those plots include the charge densities of the entire system (i.e., substrate and adsorbate) at any given voltage. On the other hand experimentally obtained constant current STM images only include surface states that are in the vicinity of the tip (< 2 Å) as it moves along the surface (raster scan). So direct comparison of calculated partial charge density to experimental STM images is not rational. For a logical comparison, we sampled the partial charge density of porphyrin/substrate at 5Å above porphyrin plane. In the present study, we plotted the constant current (iso-density) STM images of CoOEP on Au(111) and HOPG(0001) surfaces at 4 bias voltages each. The 4 bias voltages refer to 2 successive bands each in occupied (-ve bias) and unoccupied (+ve bias) states. Calculated STM images of CoOEP on Au(111) and HOPG at both +ve and –ve sample bias are depicted in Fig. 7, 8 with respective bias voltages at top right corner of each image.

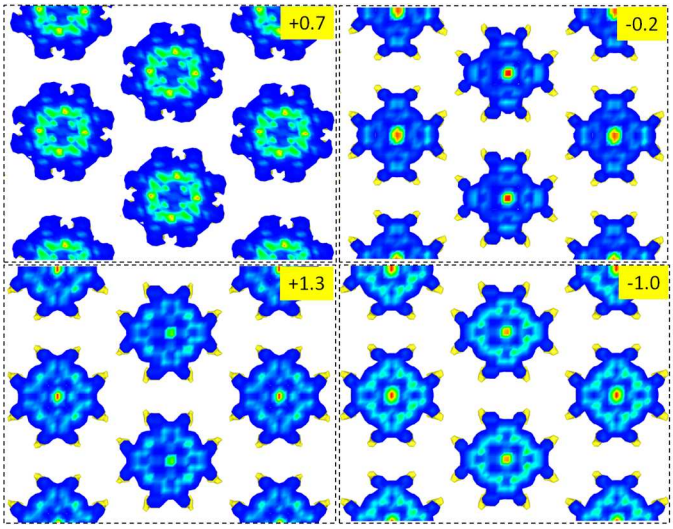

Fig. 7 Simulated STM images of CoOEP/Au(111) with respective bias voltages at the top right corner of each image. Figures on the left and right are sample biased at +ve and -ve voltages respectively. LDOS color scale: Red (high), Yellow (medium), Green (low) and Blue (zero).

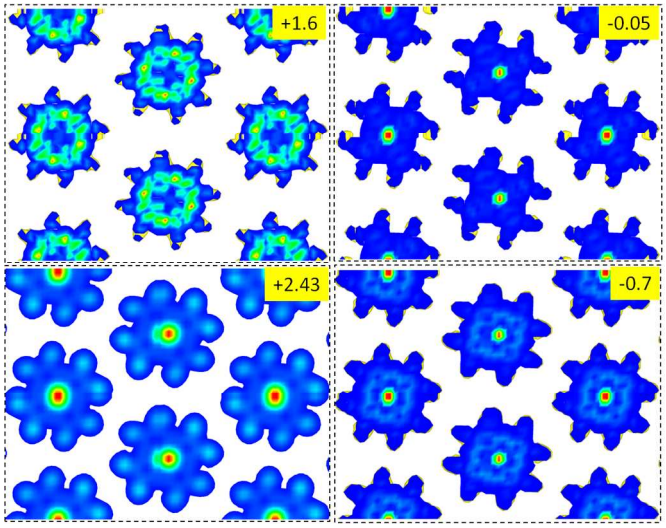

Fig. 8 Simulated STM images of CoOEP/HOPG(0001) with respective bias voltages at the top right corner of each image. Figures on the left and right are sample biased at +ve and -ve voltages respectively. LDOS color scale: Red (high), Yellow (medium), Green (low) and Blue (zero).

STM images of both Au(111) and HOPG systems look very similar in either sample bias and this is also consistent with the pDOS at the top of valence band and bottom of conduction band for CoOEP monolayer on either substrates. Some interesting comparisons between the –ve and +ve sample bias images are the clear protrusions of bonding and anti-bonding orbitals on the porphyrin backbone respectively. Also the LDOS for the cobalt atom is much more pronounced at the –ve than the +ve sample bias. The simulated images are consistent with the experimentally obtained STM images of CoOEP monolayer on Au(111)[69] and HOPG[17] substrates at –ve sample bias. Simulated STM images of CoOEP molecule on both Au(111) and HOPG show protrusions of a brighter cobalt(II) metal center and a less brighter porphyrin backbone, substituents agreeing with the experimental solid/solution STM data. *These results indicate that we can qualitatively predict the STM images of monolayers at higher bias voltages which would otherwise be difficult in an experimental setup due to substrate state interference.* Also the simulated STM images are qualitatively consistent with the experimentally observed STS spectra of cobalt and nickel porphyrins[27, 28] on metal substrates.

Summary and Conclusions

A theoretical study of cobalt(II) octaethylporphyrin (CoOEP) molecule on Au(111) and HOPG(0001) surfaces was performed using density functional theory. *For the first time we report a dispersion-DFT study of porphyrins on conducting substrates. Also for the first time, a simultaneous comparative study between different substrates and porphyrin molecules with and without dispersion has been performed.* Periodic simulations based on experimental crystal structures, scanning tunneling microscopy (STM) images and molecular DFT calculations indicate that CoOEP prefers to bind slightly strongly to HOPG(0001) than to Au(111) at the 6-fold and 3-fold center sites of the substrates, respectively. Adsorption energies of CoOEP on gold and HOPG obtained with dispersion DFT calculations agree with experimental binding energies of similar organic building blocks on metal and graphite slabs. It was also shown that porphyrins bind more strongly to gold than to HOPG.

Charge redistribution maps of both interfaces display charge localization mostly on the porphyrin molecule indicating a '*push back effect'* from the substrate. Calculations with dispersion DFT indicate a larger substrate-to-molecule charge push on Au(111)

than on HOPG. Work functions (Φ) are reduced from clean to monolayer adsorbed surfaces and the calculated values qualitatively agreed with the experimental Φ values. Calculations also show that surface dipoles are mostly responsible for the work function changes. Comparison of density of states of isolated CoOEP molecule and its monolayer on gold/HOPG substrates revealed significant orbital hybridization and band shifts. Finally, STM images were simulated using the local DOS and selected partial charge density which agreed with the experimental constant current STM data. In all the interfacial properties determined in this study, it was revealed that dispersion interactions played a critical role in altering the adsorption and charge distribution especially in Au(111) system. The present study depicts a clear picture and a thorough understanding of molecule-substrate interactions and the role of dispersion forces between porphyrin monolayers and conductive substrates.

Acknowledgements

This material is based upon work supported by the National Science Foundation under grants CHE-1058435 and CHE-1112156. Instrumentation facilities were supported by a series of NSF grants, the most current being CHE-1048600.B.C thanks Dr. Henry Pinto at Jackson State University, Jackson, MS for his help with bSKAN code.

References

1. K. M. Kadish, K. M. Smith, R. Guilard and Editors, *Handbook of Porphyrin Science with Applications to Chemistry, Physics, MaterialsScience, Engineering, Biology and Medicine: Volume 18; Applications and Materials*, World Scientific Publishing Co. Pte. Ltd., 2012.
2. K. Garg, A. Singh, C. Majumder, S. K. Nayak, D. K. Aswal, S. K. Gupta and S. Chattopadhyay, *Organic Electronics*, 2013, **14**, 1189-1196.
3. G. Sedghi, V. M. Garcia-Suarez, L. J. Esdaile, H. L. Anderson, C. J. Lambert, S. Martin, D. Bethell, S. J. Higgins, M. Elliott, N. Bennett, J. E. MacDonald and R. J. Nichols, *Nature Nanotechnology*, 2011, **6**, 517-523.
4. H. Yamada, H. Imahori, Y. Nishimura, I. Yamazaki, T. K. Ahn, S. K. Kim, D. Kim and S. Fukuzumi, *Journal of the American Chemical Society*, 2003, **125**, 9129-9139.
5. T. Wakahara, P. D'Angelo, K. i. Miyazawa, Y. Nemoto, O. Ito, N. Tanigaki, D. D. C. Bradley and T. D. Anthopoulos, *Journal of the American Chemical Society*, 2012, **134**, 7204-7206.
6. K. R. Graham, Y. Yang, J. R. Sommer, A. H. Shelton, K. S. Schanze, J. Xue and J. R. Reynolds, *Chemistry of Materials*, 2011, **23**, 5305-5312.
7. Z. Wang, Z. Li, C. J. Medforth and J. A. Shelnutt, *Journal of the American Chemical Society*, 2007, **129**, 2440-2441.
8. Z. Wang, C. J. Medforth and J. A. Shelnutt, *Journal of the American Chemical Society*, 2004, **126**, 15954-15955.
9. V. Snitka, V. Mizariene, I. Bruzaite, V. Lendraitis and M. Rackaitis, *International Journal of Nanomanufacturing*, 2010, **5**, 194-204.
10. T. Carofiglio, E. Comini, A. Gasparotto, E. Lubian, C. Maccato and G. Sberveglieri, *Journal of Nanoscience and Nanotechnology*, 2011, **11**, 3235-3244.
11. J. Otsuki, *Coordination Chemistry Reviews*, 2010, **254**, 2311-2341.
12. D. Barlow, L. Scudiero and K. W. Hipps, *Ultramicroscopy*, 2003, **97**, 47-53.
13. B. Gyarfas, B. Wiggins and K. W. Hipps, *Journal of Physical Chemistry C*, 2010, **114**, 13349-13353.
14. K. R. A. Nishida, B. C. Wiggins, K. W. Hipps and U. Mazur, *Journal of Porphyrins and Phthalocyanines*, 2011, **15**, 459-466.
15. L. Scudiero, K. W. Hipps and D. E. Barlow, *Journal of Physical Chemistry B*, 2003, **107**, 2903-2909.
16. A. Bhattarai, U. Mazur and K. W. Hipps, *Journal of the American Chemical Society*, 2014, **136**, 2142-2148.
17. B. A. Friesen, A. Bhattarai, U. Mazur and K. W. Hipps, *Journal of the American Chemical Society*, 2012, **134**, 14897-14904.
18. A. Ogunrinde, K. W. Hipps and L. Scudiero, *Langmuir*, 2006, **22**, 5697-5701.
19. L. Scudiero, D. E. Barlow and K. W. Hipps, *Journal of Physical Chemistry B*, 2002, **106**, 996-1003.
20. L. Scudiero and K. W. Hipps, *Journal of Physical Chemistry C*, 2007, **111**, 17516-17520.
21. T. Takahashi, H. Tokailin and T. Sagawa, *Physical Review B*, 1985, **32**, 8317-8324.
22. Y.-J. Yu, Y. Zhao, S. Ryu, L. E. Brus, K. S. Kim and P. Kim, *Nano Letters*, 2009, **9**, 3430-3434.
23. W. Eberhardt, I. T. McGovern, E. W. Plummer and J. E. Fisher, *Physical Review Letters*, 1980, **44**, 200-204.
24. P. G. Schroeder, C. B. France, B. A. Parkinson and R. Schlaf, *Journal of Applied Physics*, 2002, **91**, 9095-9107.
25. in *CRC Handbook of Chemistry and Physics*, Editon edn., 2008, pp. 12-114.
26. D. E. Barlow, L. Scudiero and K. W. Hipps, *Langmuir*, 2004, **20**, 4413-4421.
27. L. Scudiero, D. E. Barlow, U. Mazur and K. W. Hipps, *Journal of the American Chemical Society*, 2001, **123**, 4073-4080.
28. L. Scudiero, D. E. Barlow and K. W. Hipps, *The Journal of Physical Chemistry B*, 2000, **104**, 11899-11905.
29. A. Weber-Bargioni, W. Auwärter, F. Klappenberger, J. Reichert, S. Lefrançois, T. Strunskus, C. Wöll, A. Schiffrin, Y. Pennec and J. V. Barth, *ChemPhysChem*, 2008, **9**, 89-94.
30. T. Wolfle, A. Gorling and W. Hieringer, *Physical Chemistry Chemical Physics*, 2008, **10**, 5739-5742.
31. K. Comanici, F. Buchner, K. Flechtner, T. Lukasczyk, J. M. Gottfried, H.-P. Steinruck and H. Marbach, *Langmuir*, 2008, **24**, 1897-1901.
32. K. Flechtner, A. Kretschmann, H.-P. Steinrück and J. M. Gottfried, *Journal of the American Chemical Society*, 2007, **129**, 12110-12111.
33. T. Lukasczyk, K. Flechtner, L. R. Merte, N. Jux, F. Maier, J. M. Gottfried and H.-P. Steinrück, *The Journal of Physical Chemistry C*, 2007, **111**, 3090-3098.
34. Y. Bai, M. Sekita, M. Schmid, T. Bischof, H.-P. Steinruck and J. M. Gottfried, *Physical Chemistry Chemical Physics*, 2010, **12**, 4336-4344.
35. J. M. G. Yun Bai and Florian Buchner and Ina Kellner and Martin Schmid and Florian Vollnhals and Hans-Peter Steinrück and Hubertus Marbach and, *New Journal of Physics*, 2009, **11**, 125004.
36. W. Auwärter, K. Seufert, F. Klappenberger, J. Reichert, A. Weber-Bargioni, A. Verdini, D. Cvetko, M. Dell'Angela, L. Floreano, A. Cossaro, G. Bavdek, A. Morgante, A. P. Seitsonen and J. V. Barth, *Physical Review B*, 2010, **81**, 245403.
37. K. Seufert, M.-L. Bocquet, W. Auwärter, A. Weber-Bargioni, J. Reichert, N. Lorente and J. V. Barth, 2011, **3**, 114-119.
38. R. González-Moreno, A. Garcia-Lekue, A. Arnau, M. Trelka, J. M. Gallego, R. Otero, A. Verdini, C. Sánchez-Sánchez, P. L. de Andrés, J. Á. Martín-Gago and C. Rogero, *The Journal of Physical Chemistry C*, 2013, **117**, 7661-7668.
39. M. S. Dyer, A. Robin, S. Haq, R. Raval, M. Persson and J. Klimeš, *ACS Nano*, 2011, **5**, 1831-1838.
40. Z. Hu, B. Li, A. Zhao, J. Yang and J. G. Hou, *The Journal of Physical Chemistry C*, 2008, **112**, 13650-13655.
41. H. Kim, W.-j. Son, W. J. Jang, J. K. Yoon, S. Han and S.-J. Kahng, *Physical Review B*, 2009, **80**, 245402.
42. Z. T. Deng, H. M. Guo, W. Guo, L. Gao, Z. H. Cheng, D. X. Shi and H. J. Gao, *The Journal of Physical Chemistry C*, 2009, **113**, 11223-11227.
43. A. Terentjevs, M. P. Steele, M. L. Blumenfeld, N. Ilyas, L. L. Kelly, E. Fabiano, O. L. A. Monti and F. Della Sala, *The Journal of Physical Chemistry C*, 2011, **115**, 21128-21138.

44. L. A. Zotti, G. Teobaldi, W. A. Hofer, W. Auwärter, A. Weber-Bargioni and J. V. Barth, 2007, **601**, 2409-2414.
45. Y. Chin, D. Panduwinata, M. Sintic, T. J. Sum, N. S. Hush, M. J. Crossley and J. R. Reimers, *The Journal of Physical Chemistry Letters*, 2010, **2**, 62-66.
46. M. Linares, P. Iavicoli, K. Psychogyiopoulou, D. Beljonne, S. De Feyter, D. B. Amabilino and R. Lazzaroni, *Langmuir*, 2008, **24**, 9566-9574.
47. S. n. A. Suárez, M. H. Fonticelli, A. A. Rubert, E. de la Llave, D. n. Scherlis, R. C. Salvarezza, M. A. Martí and F. Doctorovich, *Inorganic Chemistry*, 2010, **49**, 6955-6966.
48. P. M. Oppeneer, P. M. Panchmatia, B. Sanyal, O. Eriksson and M. E. Ali, 2009, **84**, 18-29.
49. V. Barone, M. Casarin, D. Forrer, S. Monti and G. Prampolini, *The Journal of Physical Chemistry C*, 2011, **115**, 18434-18444.
50. H. J. Jens Brede and Mathieu Linares and Stefan Kuck and Jörg Schwöbel and Alessandro Scarfato and Shih-Hsin Chang and Germar Hoffmann and Roland Wiesendanger and Roy Lensen and Paul, *Nanotechnology*, 2009, **20**, 275602.
51. P. Donovan, A. Robin, M. S. Dyer, M. Persson and R. Raval, *Chemistry – A European Journal*, 2010, **16**, 11641-11652.
52. S. Grimme, J. Antony, S. Ehrlich and H. Krieg, *The Journal of chemical physics*, 2010, **132**, 154104.
53. S. Grimme, *Wiley Interdisciplinary Reviews: Computational Molecular Science*, 2011, **1**, 211--228.
54. J. Klimeš, D. R. Bowler and A. Michaelides, *Physical Review B*, 2011, **83**, 195131.
55. G. Kresse and J. Furthmüller, *Computational Materials Science*, 1996, **6**, 15-50.
56. G. Kresse and J. Furthmüller, *Physical Review B*, 1996, **54**, 11169.
57. G. Kresse and J. Hafner, *Physical Review B*, 1993, **47**, 558-561.
58. G. Kresse and D. Joubert, *Physical Review B*, 1999, **59**, 1758.
59. P. E. Blöchl, *Physical Review B*, 1994, **50**, 17953.
60. J. P. Perdew, K. Burke and M. Ernzerhof, *Physical Review Letters*, 1996, **77**, 3865.
61. W. Kohn and L. J. Sham, *Physical Review*, 1965, **140**, A1133-A1138.
62. R. B. a. A. M. Jiří Klimeš and David, *Journal of Physics: Condensed Matter*, 2010, **22**, 022201.
63. K. Lee, É. D. Murray, L. Kong, B. I. Lundqvist and D. C. Langreth, *Physical Review B*, 2010, **82**, 081101.
64. H. J. Monkhorst and J. D. Pack, *Physical Review B*, 1976, **13**, 5188.
65. J. Tersoff and D. R. Hamann, *Physical Review B*, 1985, **31**, 805-813.
66. J. Tersoff and D. R. Hamann, *Physical Review Letters*, 1983, **50**, 1998-2001.
67. A. H. Krisztián Palotás and Werner, *Journal of Physics: Condensed Matter*, 2005, **17**, 2705.
68. Wyckoff and R. W. G., *Crystal Structures*, 2 edn., Interscience Publishers, New York, New York, 1963.
69. S. Yoshimoto, J. Inukai, A. Tada, T. Abe, T. Morimoto, A. Osuka, H. Furuta and K. Itaya, *The Journal of Physical Chemistry B*, 2004, **108**, 1948-1954.
70. D. E. Goldberg and K. M. Thomas, *Journal of the American Chemical Society*, 1976, **98**, 913-919.
71. R. Dronskowski *Computational Chemistry of Solid State Materials: A Guide for Materials Scientists, Chemists, Physicists and Others*, 1 edn., Wiley-VCH Verlag GmbH & Co KGaA, Weinheim, Germany, 2005.
72. R. A. Evarestov, *Quantum Chemistry of Solids: LCAO Treatment of Crystals and Nanostructures*, Springer, Berlin, Heidelberg, New York.
73. D. Karhanek, *Ph.D. Dissertation: Self-Assembled Monolayers Studied by Density-Functional Theory* University of Vienna, Vienna, Austria, 2010.
74. C. Kittel, *Introduction to Solid State Physics*, 8 edn., John Wiley & Sons, Inc, Hoboken, NJ, USA, 2005.
75. V. Coropceanu, J. Cornil, D. A. da Silva Filho, Y. Olivier, R. Silbey and J.-L. Brédas, *Chemical Reviews*, 2007, **107**, 926-952.
76. A. Tkatchenko, L. Romaner, O. T. Hofmann, E. Zojer, C. Ambrosch-Draxl and M. Scheffler, *MRS Bulletin*, 2010, **35**, 435-442.
77. G. L. Perlovich, O. A. Golubchikov and M. E. Klueva, *Journal of Porphyrins and Phthalocyanines*, 2000, **4**, 699-706.
78. K. Toyoda, I. Hamada, L. Kyuho, S. Yanagisawa and Y. Morikawa, *Journal of Chemical Physics*, 2010, **132**, 134703.
79. G. Li, I. Tamblyn, V. R. Cooper, H.-J. Gao and J. B. Neaton, *Physical Review B*, 2012, **85**, 121409.
80. J. Lüder, B. Sanyal, O. Eriksson, C. Puglia and B. Brena, *Physical Review B*, 2014, **89**, 045416.
81. S. D. Chakarova-Käck, E. Schröder, B. I. Lundqvist and D. C. Langreth, *Physical Review Letters*, 2006, **96**, 146107.
82. D. Künzel, K. Tonigold, J. Kučera, M. Roos, H. E. Hoster, R. J. Behm and A. Groß, *ChemPhysChem*, 2011, **12**, 2242-2245.
83. J. Ziroff, P. Gold, A. Bendounan, F. Forster and F. Reinert, 2009, **603**, 354-358.
84. C. Struzzi, M. Scardamaglia, M. Angelucci, L. Massimi, C. Mariani and M. G. Betti, *Il Nuovo Cimento C*, 2013, **36**, **51-57**.
85. M. Scardamaglia, C. Struzzi, S. Lizzit, M. Dalmiglio, P. Lacovig, A. Baraldi, C. Mariani and M. G. Betti, *Langmuir*, 2013, **29**, 10440-10447.
86. M. Mura, A. Gulans, T. Thonhauser and L. Kantorovich, *Physical Chemistry Chemical Physics*, 2010, **12**, 4759-4767.
87. H. L. Skriver and N. M. Rosengaard, *Physical Review B*, 1992, **46**, 7157-7168.
88. P. S. Bagus, V. Staemmler and C. Wöll, *Physical Review Letters*, 2002, **89**, 096104.
89. S. Braun, W. R. Salaneck and M. Fahlman, *Advanced Materials (Weinheim, Germany)*, 2009, **21**, 1450-1472.
90. Y. Gao, *Materials Science & Engineering, R: Reports*, 2010, **R68**, 39-87.
91. N. Koch, *Physica Status Solidi RRL: Rapid Research Letters*, 2012, **6**, 277-293.
92. N. Koch, *ChemPhysChem*, 2007, **8**, 1438-1455.
93. G. Heimel, F. Rissner and E. Zojer, *Advanced Materials (Weinheim, Germany)*, 2010, **22**, 2494-2513.
94. G. Heimel, L. Romaner, E. Zojer and J.-L. Bredas, *Accounts of Chemical Research*, 2008, **41**, 721-729.
95. G. Heimel, L. Romaner, E. Zojer and J.-L. BrÃ©das, *Nano Letters*, 2007, **7**, 932-940.
96. B. Chilukuri and T. R. Cundari, *Surface Science*, 2012, **606**, 1100-1107.
97. B. Chilukuri and T. R. Cundari, *The Journal of Physical Chemistry C*, 2011, **115**, 5997-6003.
98. T. R. Cundari, B. Chilukuri, J. M. Hudson, C. Minot, M. A. Omary and H. Rabaa, *Organometallics*, 2010, **29**, 795-800.
99. A. Biller, I. Tamblyn, J. B. Neaton and L. Kronik, *Journal of Chemical Physics*, 2011, **135**, 164706.
100. T. Körzdörfer, S. Kümmel, N. Marom and L. Kronik, *Physical Review B*, 2009, **79**, 201205.
101. G. Heimel, L. Romaner, J.-L. Brédas and E. Zojer, 2006, **600**, 4548-4562.
102. L. Zhu, V. Coropceanu, Y. Yi, B. Chilukuri, T. R. Cundari and J.-L. Brédas, *The Journal of Physical Chemistry Letters*, 2013, **4**, 2186-2189.
103. J. Bardeen, *Physical Review*, 1947, **71**, 717-727.
104. J. Tersoff, *Physical Review Letters*, 1984, **52**, 465-468.
105. H. Vázquez, F. Flores, R. Oszwaldowski, J. Ortega, R. Pérez and A. Kahn, *The Ninth International Conference on the Formation of Semiconductor Interfaces*, 2004, **234**, 107-112.
106. L. Calliari, S. Fanchenko and M. Filippi, 2007, **45**, 1410-1418.

TOC Graphic:

Implication of dispersion interactions on geometric, adsorption and electronic properties of porphyrin monolayer on conductive surfaces using density functional theory.